Iranian Journal of Science and Technology, Transactions of Civil Engineering
https://doi.org/10.1007/s40996-023-01153-3

RESEARCH PAPER

Extreme Learning Machine for Estimation of the Engineering Properties of Self-Compacting Mortar with High-Volume Mineral Admixtures

Kazim Turk[1] · **Ceren Kina**[2] · **Harun Tanyildizi**[3]

Received: 14 January 2023 / Accepted: 21 May 2023
© The Author(s), under exclusive licence to Shiraz University 2023

Abstract
The utilization of supplementary cementitious materials obtained from industrial by-products or wastes is one of the most effective ways to minimize the costs as well as environmental impact associated with cement production. This work investigated the effects of the replacement of Portland cement (PC) with (25, 30, 35 and 40%) fly ash (FA) and (5, 10, 15, and 20%) silica fume (SF) by weight as binary and ternary blends on the compressive strength (f_c) and flexural strength (f_{ft}) of self-compacting mortars (SCMs) at 28 and 91 curing days. Extreme learning machine (ELM), support vector regression (SVR), artificial neural network (ANN), and decision tree (DT) models were devised to predict these strengths of SCMs containing high-volume mineral admixture (HVMA). The selected input variables were the number of curing days, water-cementitious material (W/CM), PC, FA, SF, and sand contents, while the f_c and f_{ft} were the output variables. ANOVA results show that the curing time was the most effective parameter for determining both strengths. The results also indicated that ELM achieved superior performance for the prediction of f_c and f_{ft} of SCMs with HVMA compared to SVR, ANN, and DT due to having the highest coefficient of determination values of 0.9802 for both strengths.

Keywords Fly ash · Silica fume · Strengths · Machine learning · ANOVA analysis

1 Introduction

1.1 Background

The most commonly used construction material is cement, but unfortunately, it is one of the highest producers of carbon dioxide emissions (Xiao et al. 2019). That is, four billion tons of cement are produced in a year, and the production process of cement causes seven percent of all carbon dioxide emissions to the atmosphere (Benhelal et al. 2013). During the manufacturing of Portland cement (PC), the calcination of calcium oxide is the main cause of the production of carbon dioxide (Barcelo et al. 2014; Kajaste and Hurme 2016). As a consequence of environmental awareness, the use of recycled or industrial by-products in concrete production is recommended and has become widespread. PC can be replaced by waste materials from industrial processes such as granite powder (Chajec 2021), ground granulated blast furnace slag (Czarnecki et al. 2021), fly ash (FA) (Turk and Kina 2018), and silica fume (SF) (Benli et al. 2018). The utilization of these supplementary raw materials reduces the use of naturally mined materials and the wastes disposed of in landfills. This will not only improve the durability and performance of concrete, but also reduce the impact of the construction industry on the natural environment due to a reduction in its carbon footprint.

1.2 Self-Compacting Mortar

Concrete material is the second most commonly utilized material after water on the Earth (Farooq et al. 2020). Due to the beneficial properties of concrete with regards to strength, durability, fire resistance, porosity, stiffness, hardness, and

✉ Ceren Kina
ceren.kina@ozal.edu.tr

[1] Department of Civil Engineering, Engineering Faculty, Inonu University, Malatya, Türkiye

[2] Department of Civil Engineering, Faculty of Engineering and Natural Sciences, Malatya Turgut Ozal University, Malatya, Türkiye

[3] Department of Civil Engineering, Technology Faculty, Firat University, Elazig, Türkiye

Published online: 15 June 2023

density, it is used as a building material all over the world. Self-compacting concrete (SCC) is a special type of concrete that has the ability to flow with its weight through congested reinforcement without applying any vibration because of its excellent deformability, while showing no bleeding or segregation. Thus, SCC requires high fluidity and moderate viscosity. The passing ability, filling capacity, and resistance to segregation are the main fresh state properties of SCC. In order to achieve these properties, a large amount of fine materials and high-performance water-reducing additives or viscosity modifiers must be used (Madandoust and Mousavi 2012).

The use of pozzolanic or inert supplementary cementitious materials has a positive effect on the environment due to the reduction in cement production (Anjos et al. 2020; Diniz et al. 2022; Larissa et al. 2020). In addition, using industrial wastes such as FA and SF is a solution to offset the increased cost caused by the use of chemical admixture and high cementitious material (Jalal et al. 2015). In addition to these materials, the pozzolanic materials contribute to increased durability by reducing permeability and shrinkage (Larissa et al. 2020). In the literature, there have been many studies (Turk et al. 2020, 2021, 2022; Türk and Kına 2017) using waste materials in PC replacement as a pozzolan.

There is a common idea that when the content of PC is reduced, it also causes a decrease in the strength of concrete. However, the use of supplementary cementitious materials with appropriate mix proportions can affect the consumption of calcium hydroxide resulting in the improvement of hardness and durability properties of concrete. Many researchers (Anjos et al. 2020; Wongkeo et al. 2014) found measured the compressive strength (f_c) of 32 MPa, 61 MPa, and 71 MPa at 28 days for specimens having PC content of 150 kg/m^3, 180 kg/m^3, and 220 kg/m^3, respectively.

The use of FA as a replacement for PC leads to many advantages including low energy consumption and water demand, improving strength and durability, and decreasing gas emissions (Bagheri et al. 2013). Nevertheless, it was found from some studies (Megat Johari et al. 2011; Siddique 2011) that the concretes/mortars with only FA as binary develop lower strength at early ages. In order to minimize the drawbacks of mineral admixtures, in many studies (Falmata et al. 2020; Turk 2012; Turk et al. 2013; Turk and Kina 2018), FA has been used in ternary blends with SF, which had a highly pozzolanic reaction. This leads to a reduction in bleeding as well as enhanced pozzolanic activity. Moreover, other research (Falmata et al. 2020; Wongkeo et al. 2014) showed that using an appropriate amount of SF and FA as ternary blends provides noticeable improvement in the strength of mortar and concrete.

The strength of concrete, such as in compressive and flexural modes, is affected by many parameters because concrete is a heterogeneous material including binders, aggregates, water, and admixtures. The ingredients and their mix proportions, such as type and amount of binders, size of aggregate, water-binder ratio, etc., cause differences in the strengths of concrete (Cotsovos and Pavlović 2008). Therefore, the strengths of concrete can commonly be evaluated in laboratory conditions by using standard procedures, but these tests are time-consuming and uneconomical as they are costly. Thus, it is important to predict the strength of concrete accurately. Recently, machine learning (ML) algorithms were devised for the prediction of mechanical properties in concrete (Feng et al. 2020). They help in forecasting the fresh properties, durability, as well as strengths of concrete with accuracy and precision (Ahmad et al. 2021b; Farooq et al. 2021; Kina et al. 2021, 2022a, b).

1.3 Machine Learning Techniques

Nowadays, many ML techniques, including artificial neural networks (ANNs), support vector regression (SVR), extreme learning machines (ELMs), decision trees (DTs), random forest (RF), and genetic engineering programming (GEP) are widely used to predict the strength of traditional concrete, SCC and cement mortar. Among these techniques, SVMs can better deal with nonlinear regression. Therefore, SVM models can achieve better solutions and have well-generalized ability (Lv et al. 2013). An ANN has universal approximation capability and is an effective technique to develop the input and output relations for complex problems (Gupta et al. 2019). ELMs are a relatively new learning method. An ELM has a fast learning speed and good generalization performance. RF selects the feature variables randomly within the given parameters while DT uses entire databases with the variable of its interest, and both of these techniques behave like a tree structure (Dou et al. 2019). GEP is one of the other ML techniques that mimics Darwinian evolution (Zhang and Tsai 2003).

The use of ML algorithms in civil engineering has increased significantly in recent years due to the prediction of mechanical properties with high accuracy. In the study of Su et al. (2021), multiple linear regression (MLR), SVM, and ANN models were devised to estimate the interfacial bond strength between concrete and fiber-reinforced polymers. It was found that SVM predicted the results with the best accuracy and efficiency. The f_c of concrete was predicted by Güçlüer et al. (2021) via DT, ANN, SVR, and linear regression models. Their analysis showed that the correlation coefficient and mean absolute error were the best at 0.86 and 2.59%, respectively, for the DT algorithm. Jueyendah et al. (2021) proposed an SVM method with a radial basis function for the prediction of the f_c and flexural strength (f_{ft}) of cement mortar due to the higher correlation coefficient values with 0.9987 and 0.9970, respectively. In the study of Sultana et al. (2020), response surface methodology, ANN,

and SVR models were used to predict the strength of jute-fiber-reinforced concrete composites and it was noted that the SVR had the lowest mean absolute error (MAE) and root mean square error (RMSE). Azimi-Pour et al. (2020) predicted the f_c of SCC with high FA content by using the SVR model based on a radial basis kernel function with an *R*-squared value of 0.9932. Yaseen et al. (2018) devised multivariable adaptive regression spline, ELM, SVR, and M5 tree models for the estimation of the f_c of lightweight foamed concrete and noted that the ELM had superior performance. Al-Shamiri et al. (2019) estimated the f_c of high-strength concrete using ELM and ANN models. They stated that the ELM model had extremely fast learning speed and that during the training process, no iteration was required.

2 Research Significance

There are two points of novelty/significance in this research. The first one is to carry out an experimental work to assess the effects of using a high volume of mineral admixtures in binary (PC + FA and PC + SF) and ternary blends (PC + FA + SF) into SCMs. The aim was to understand the synergistic effects of FA and SF in SCM as well as to produce SCC with low PC content for environmental awareness. The use of high-volume mineral admixture is one of the most important ways to achieve sustainability in construction due to its advantages in terms of cost, performance, durability and environmental impact. However, the preparation of mixtures having different contents of mineral admixtures and their binary and ternary blends need comprehensive laboratory conditions to determine mechanical properties. On the other hand, prediction models can be an alternative solution to minimize cost, labor and time investments. Within this scope, the second point of novelty of this research is to develop an ELM model to predict the f_c and f_{ft} of SCMs with high-volume mineral admixture including binary and ternary blends of FA and SF, and to give a different point of view to the literature. As mentioned in the previous section, there have been many studies (Azimi-Pour et al. 2020; Güçlüer et al. 2021; Jueyendah et al. 2021; Su et al. 2021; Sultana et al. 2020) that used ML algorithms to estimate the strengths of mortar/concrete. On the other hand, there have been limited studies (Al-Shamiri et al. 2019; Yaseen et al. 2018) that devised ELM models to predict the strengths of concrete/mortar, so one goal was to investigate the utility of ELM-based models in the field of civil engineering. The focus of this work is to predict the compressive and flexural strengths of SCMs having binary and ternary blends of FA and SF using an ELM and also to compare the prediction results with other ML approaches including SVR, ANNs, and DTs. Moreover, this work investigated the role of the experimental variables using analysis of variance (ANOVA) and also derived a multiple linear regression (MLR) model. Thus, the input parameters defined in each ML model were utilized to predict the output parameters, and adequate MLR equations were assessed according to the performance evaluation parameters.

3 Methodology of Devised Machine Learning (ML) Models

This section describes the devised ML models to predict the f_c and f_{ft} of SCMs with binary and ternary blends of FA and SF. MATLAB software was used to run the prediction models. The forecasting of the strengths was made by using ELM, SVR, ANN, and DT models.

The training procedure of the ML algorithms was started by checking for extreme values. The outliers would not represent the overall behavior of the system, so it is important to reduce such errors. Then, in order to identify cause-effect relationships and avoid selection bias, the data set was transformed before separating the data into training–testing data sets (Salami et al. 2020). After that, the transformed data sets were used in the ML algorithms. The training set was utilized for model training, and finally, the model was applied to the testing data set to evaluate its predictive performance.

In this study, SVR, ANN and DT models were devised due to their popularity as well as their high prediction potential (Ahmad et al. 2021a; Asteris and Mokos 2020; Güçlüer et al. 2021; Tanyildizi 2021; Tanyildizi et al. 2020). On the other hand, ELM models are not common in the field of civil engineering. Therefore, in order to investigate the utility of ELMs in the prediction of the hardened properties of SCMs with high mineral content, the prediction results obtained from ELM, SVR, ANN, and DT models were compared by using a Taylor diagram and the performance evaluation metrics described herein.

3.1 Extreme Learning Machine (ELM)

The ELM is a popular estimation method used for training single-layer feed-forward neural networks (SLFNs). A classification task is aimed in ELM with zero error, and the weights of the input layer are appointed randomly. Furthermore, the weights of the hidden layer are determined analytically in accordance with the input properties and class label relationships (Alçin et al. 2015; Bin et al. 2006). Random values are assigned to hidden layer's weights and the output weights were computed by using the minimum-norm least-squares method, so the ELM does not need an optimization step.

A three-step procedure is used to model data using the ELM. The first one is to create a SLFN. The second is to select biases of the network and the weights of the hidden

layer randomly. The last is to estimate the weights of the output by inverting the output matrix of the hidden layer (Al-Shamiri et al. 2019). Figure 1 shows the architecture of the ELM model.

Suppose a set of N training samples as $(x_i, y_i), i = 1, \ldots, N$ where $x_i = [x_{i1}, x_{i2} \ldots x_{in}]^T$ and $y_i = [y_{i1}, y_{i2} \ldots y_{im}]^T \in R^m$. The output with M hidden neurons and $g(x)$ activation function is expressed as follows (Bin 2003):

$$\sum_{i=1}^{M} B_i g(w_i \times x_i + b_j) = o_j, \quad j = 1, \ldots, N \tag{1}$$

where $B_i = [B_{i1}, B_{i2} \ldots B_{im}]^T$ is the weight vector between i-th hidden neuron and output neuron, $w_i = [w_{i1}, w_{i2} \ldots w_{in}]^T$ is the weight vector between i-th hidden neuron and input neuron, b_i is the threshold value of the i-th hidden neuron, and o_i is the output vector.

In a standard ELM model (Gao et al. 2019):

$$\sum_{i=1}^{M} B_i g(w_i \times x_i + b_j) = y_j, \quad j = 1, \ldots, N \tag{2}$$

Equation 2 can be written as:

$$\mathrm{PS} = H \tag{3}$$

in which:

$$P = \begin{bmatrix} g(w_1 \times x_1 + b_1) & \cdots & g(w_N \times x_1 + b_N) \\ \vdots & \cdots & \vdots \\ g(w_1 \times x_M + b_1) & \cdots & g(w_N \times x_1 + b_N) \end{bmatrix}_{N \times M} \tag{4}$$

$$S = \begin{bmatrix} S_1^T \\ \vdots \\ S_M^T \end{bmatrix}_{M \times 1} \tag{5}$$

$$H = \begin{bmatrix} H_1^T \\ \vdots \\ H_N^T \end{bmatrix}_{N \times 1} \tag{6}$$

The hidden layer output matrix P is calculated based on the input data set, the weights of the input layer, activation functions and biases (Bin 2003). H is the training data set. The output weights S can be calculated by using Eq. (7) (Bin et al. 2006).

$$\mathrm{S} = P^{+}H \tag{7}$$

in which P^+ is the Moore–Penrose generalized inverse of matrix P. The algorithm of the ELM model is summarized as follows (Lan et al. 2010);

- Input: Given N training samples, nonlinear activation function $g(x)$ and SLFN with M hidden neurons
- The input weights and biases of hidden neurons are initiated randomly,
- The hidden layer output matrix (P) is calculated,
- The output weights (S) are obtained by using the least-squares method.

3.2 Support Vector Regression (SVR)

The SVR model is a supervised learning approach to solve high-dimensional optimization problems. It involves suitable generalization, precision and accuracy as well as powerful theoretical concepts (Cristianini and Shawe-Taylor 2000). In order to map the input space through the feature domain, a kernel function is used. By reducing the error function, it can yield a global solution. Compared to other gradient based models, SVR is widely employed especially

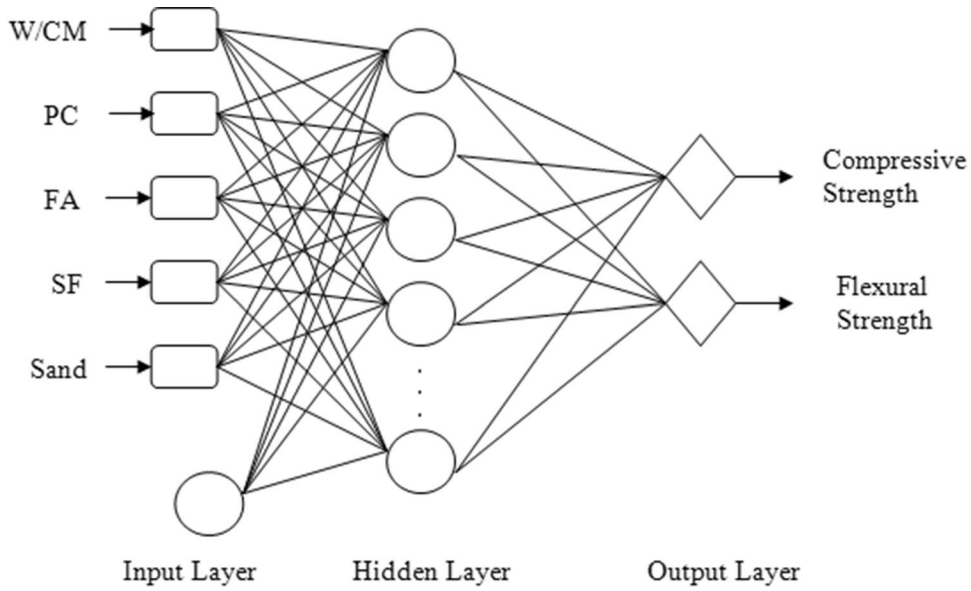


Fig. 1 The architecture of the ELM model used in this study

due to providing higher modeling accuracy and a faster training process (Cherkassky and Mulier 2006). It also shows good resistance against overfitting and works well on small data sets.

Assume a data set of N training samples as $\{(x_i, y_i), (x_i, y_i), \ldots, (x_i, y_i)\}$ where x_i is an l-dimensional real director and y_i is a scalar regression value. The equation of regression can be expressed as below:

$$f(x) = w \cdot \varphi(x) + b \tag{8}$$

in which w is the weight vector, $\varphi(x)$ is the nonlinear mapping function and b is bias. If the deviation between y_i and $f(x_i)$ is less than the largest tolerance error (ε), the function of $f(x_i)$ is found. Figure 2 shows the nonlinear SVR with an ε-insensitive loss function. To build $f(x)$, only the data placed on or outside of the $\pm\varepsilon$ parts are used. ξ_i^* and ξ_i are slack variables which evaluate the upper and lower bounds.

The nonlinear SVR can be expressed as follows (Yuvaraj et al. 2013):

$$\begin{aligned}\max[w(\alpha, \alpha*)] = \max &\left[\sum_{i=1}^{n} y_i(\alpha_i^* - \alpha_i) - \in \sum_{i=1}^{n}(\alpha_i^* + \alpha_i)\right.\\ &\left. - \frac{1}{2}\sum_{ij=1}^{n}(\alpha_i^* - \alpha_i)(\alpha_i^* - \alpha_i)\{(x_i)(x_j)\}\right]\\ &\alpha;\alpha* \quad \alpha;\alpha*\end{aligned}$$

$$\text{subjected to} \quad \begin{cases}\sum_{i=1}^{n}(_i^* - _i) = 0 \;\; i = 1, \ldots n\\ 0 < \alpha_i^*, \qquad \alpha_i \le 0\end{cases} \tag{9}$$

According to Mercer's condition (Vapnik 1999), the inner product of $\Phi(x_i)\Phi(x_j)$ is replaced by a kernel function $K(x_i, x_j)$. Thus, in input space, a simple arithmetic computation is used instead of a complex computation in the feature space. For this reason, Eq. (9) can be rewritten as follows:

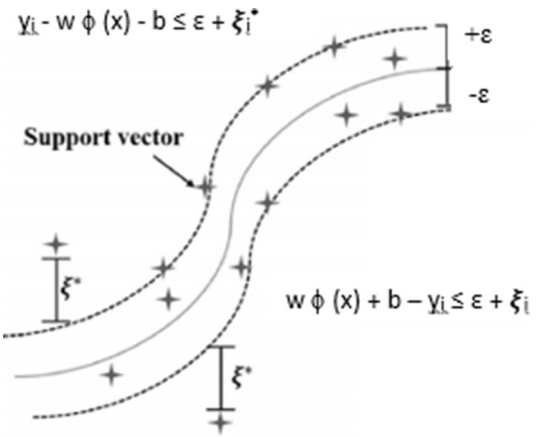


Fig. 2 The nonlinear SVR with ε-insensitive loss function

$$\begin{aligned}\max[w(\alpha, \alpha*)] = \max &\left[\sum_{i=1}^{n} y_i(\alpha_i^* - \alpha_i) - \in \sum_{i=1}^{n}(\alpha_i^* + \alpha_i)\right.\\ &\left. - \frac{1}{2}\sum_{ij=1}^{n}(\alpha_i^* - \alpha_i)(\alpha_i^* - \alpha_i)K(x_i x_j)\right]\\ &\alpha;\alpha* \quad \alpha;\alpha*\end{aligned} \tag{10}$$

$$K(x, y) = \exp\{-y\|x - y\|^2\} y \ge 0 \tag{11}$$

where x and y were the training pattern and test pattern, respectively. This function was used because it is the most common and suitable kernel function as can be seen from the literature (Jueyendah et al. 2021; Karimipour et al. 2019). The optimal values of the parameters of C and ε were determined by trial and error.

3.3 Artificial Neural Network (ANN)

The ANN is a soft-computing technique which is inspired by the biological nervous system including number of cells referred to as neurons. These interconnected simple computational nodes (neurons) are usually arranged into groups to form layers in the network and to obtain a response, which is called the output, from a series of inputs (Shahin et al. 2009). The neurons are connected to each other through connection weights. Each neuron also has an activation function. The numbers of neurons in the input and output layers depend on the variables in the models. After being passed into the artificial neuron, input data is processed using mathematical functions and output data is obtained. To simulate the neurons, weights are attributed to the input parameters before entering the input data into the neuron. Modeling with ANNs required three main stages: (a) the architecture of the model must be determined; (b) the training algorithm for the learning phase must be defined; (c) the mathematical function must be appointed. The organization of the artificial neurons and the information flows within the network were described by the architecture of ANN model. The training phase of the ANN is a function minimization problem which means that the error function is minimized. The determination of the mathematical function is also so important because the behavior of neurons is defined by the summation of their activation functions (Asteris and Mokos 2020). Therefore, ANN is composed of inputs, weights, sum function, activation function and outputs.

Suppose a set of n input data applied to the artificial neurons as $X = (X_1, X_2, X_3, \ldots X_n)$ and the output of the neurons is as follows

$$u = \sum_{j=0}^{m} x_j w_j - b \tag{12}$$

$$V = f(u) \tag{13}$$

in which w_j is the weight of the neural model, x_j is the input data and b is a bias. In the devised ANN model, the most appropriate activation function and structure for ANN must be selected. The architecture of the ANN model is shown in Fig. 3.

3.4 Decision Tree (DT)

The DT is a ML method which creates an efficient model for regression and data classification (Karbassi et al. 2014). There are three parts in the classification of the decision tree that can be thought of as implementing an "if–then" strategy; (i) the selection of features, (ii) construction of the model, and (iii) pruning of the DT. The algorithm is developed by splitting a data set into branch-like segments so the decision tree involves nodes and directed edges.

In the DT model, the internal nodes stand for the features, the branches show conclusion rules, and the leaf nodes form the outcome. As shown in Fig. 4, in the classification procedure, at first, the feature from the root node is selected by the decision tree. Then, the root node is divided into two sub-nodes. This process continued until all the sub-nodes are leaf nodes. The sub-nodes have multiple branches, but leaf nodes do not have branches that are considered as the output. The DT model reflects a tree-like structure as it starts with the root node and is distributed according to the number of branches (Ben Chaabene et al. 2020). The branches underneath the root nodes are formed by the decision rules which describe the relationship between inputs and targets. Decision rules predict the values of the observations that contain values for the inputs. With the developed algorithm, the error between the target and predicted value is found at each split point. The variable with the least value for the fitness function is chosen as a split point and this process is repeated.

4 Experimental Program

4.1 Materials and Mix Design

Materials utilized in this experimental work were as follows: CEM I 42.5R PC with a specific gravity of 3.1 and natural river sand (with 2 mm max size, the water absorption rate and relative density of 1.96% and 2.63 g/cm^3, respectively). The supplementary cementitious materials used were SF and FA with specific gravity of 2.2 and 2.08, respectively. The fresh properties of SCMs were determined by using different content of SF and FA as well as a modified high range water reducing additive (HRWRA) with a specific gravity of 1.08. The physical properties and chemical compositions of the cementitious materials were shown in Table 1.

The experimental program of this study aimed to assess the effect of the binary and ternary blends of SF and FA

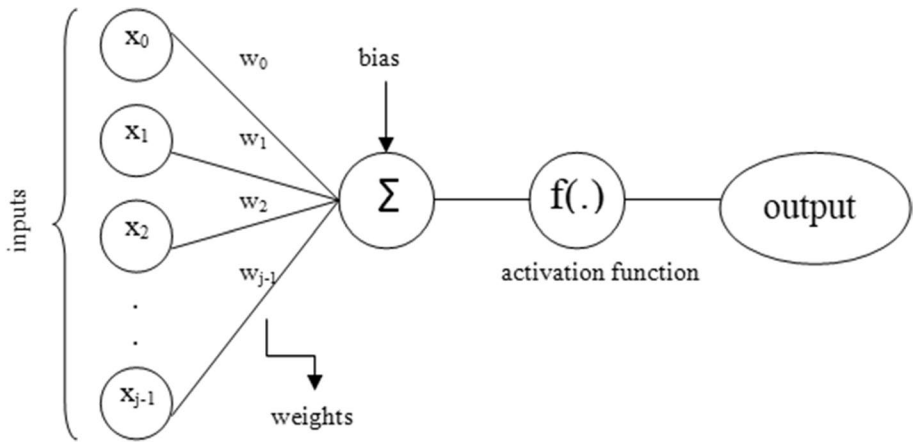


Fig. 3 The architecture of the ANN model

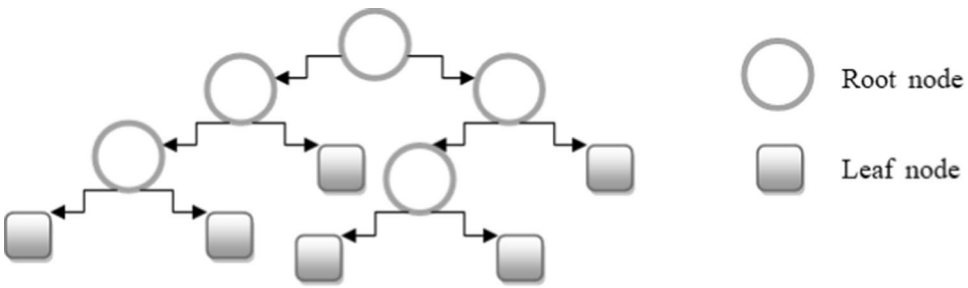


Fig. 4 Schematic diagram of DT model

Table 1 The chemical compositions and physical properties of cementitious materials

Cementitious Materials	Composition (%)						Specific surface area (cm^2/g)
	SiO_2	Al_2O_3	Fe_2O_3	CaO	MgO	SO_3	LOI	
PC	20.2	5.8	3.23	64.1	–	2.66	2.58	3484
FA	58.82	19.65	10.67	2.18	3.92	0.48	0.91	3812
SF	91	0.58	0.24	0.71	0.33	–	1.84	96.5% < 45 mm

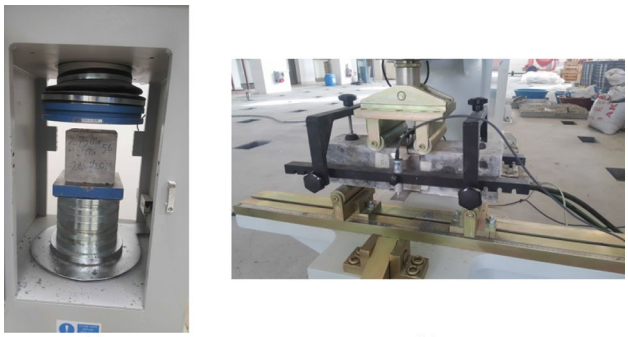
replaced by PC by weight. In light of this fact, one control mixture with only PC as a binder and 24 SCMs incorporating binary and ternary cementitious blends were produced. The binary SCMs included either FA (PC + FA) or SF (PC + SF) as a replacement of some proportion of PC, while ternary SCMs were prepared by adding both FA and SF as well as PC. The replacement ratios for SF were 5%, 10%, 15%, 20% while those of FA were 25%, 30%, 35%, 40% by weight of PC. As shown in Table 2, the total binder content was kept constant as 640 kg/m^3 while the W/CM ratio was arranged between 0.41 and 0.50. It is noteworthy that the use of the same W/CM ratio for all mixtures was not possible due to the roughness and high surface area of the mineral additions.

4.2 Preparation and Testing of Specimens

The same processes were applied to achieve uniformity and homogeneity in all mixtures for the production of all SCMs. The binders and sand were mixed for a minute. Then, HRWRA with mixing water was added into the mixer and mixed for four minutes. The EFNARC (2002) recommendations were satisfied by changing the dosage of HRWRA. Within this scope, the SCMs were designed to achieve a slump-flow diameter of 25 ± 1. In the hardened state, f_c and f_{ft} tests were conducted at 28 and 91 curing days according to ASTM C39 (2020) and ASTM C09 (2000) standards, respectively. Observing Fig. 5, the f_c test was performed using cube samples having dimensions

Table 2 Mortar mixture proportions

Mixture codes	PC (kg/m^3)	SF (kg/m^3)	FA (kg/m^3)	W/CM	Sand (kg/m^3)	HRWRA (kg/m^3)
Control	640	0	0	0.45	1227	6.75
FA25	480	0	160	0.43	1194	6.75
FA30	448	0	192	0.43	1181	6.75
FA35	416	0	224	0.43	1168	6.75
FA40	384	0	256	0.43	1155	6.75
SF5	608	32	0	0.44	1230	8
SF10	576	64	0	0.45	1203	8
SF15	544	96	0	0.47	1159	8
SF20	512	128	0	0.50	1106	8
SF5FA25	448	32	160	0.43	1174	8
SF5FA30	416	32	192	0.41	1193	8
SF5FA35	384	32	224	0.41	1185	8
SF5FA40	352	32	256	0.41	1180	8
SF10FA25	416	64	160	0.43	1169	8
SF10FA30	384	64	192	0.42	1174	8
SF10FA35	352	64	224	0.41	1166	8
SF10FA40	320	64	256	0.41	1164	8
SF15FA25	384	96	160	0.44	1148	8
SF15FA30	352	96	192	0.43	1143	8
SF15FA35	320	96	224	0.43	1140	8
SF15FA40	288	96	256	0.42	1143	8
SF20FA25	352	128	160	0.48	1072	8
SF20FA30	320	128	192	0.47	1069	8
SF20FA35	288	128	224	0.47	1061	8
SF20FA40	256	128	256	0.46	1056	8



(a) (b)

Fig. 5 The test setup for **a** compressive strength test and **b** flexural strength test

of $100 \times 100 \times 100$ mm^3 and a loading rate of 6 kN/s. The f_{ft} test was carried out via four-point bending on beams of $100 \times 100 \times 400$ mm. The rate of loading was 0.003 mm/s. The average values of the results of three test specimens prepared for each mixture were calculated.

5 Performance Evaluation of Devised Machine Learning (ML) Models

Calculating the error rates between the actual and predicted values obtained from ML algorithms is valuable in terms of understanding the success of the method used. In this study, the error rates were revealed by evaluating the error between the predicted values obtained by the ML models and the actual values in the training data set. The predictability capacity of the developed ML algorithms was evaluated using six statistical indicators that describe model fitting. The metrics used to appraise the accuracy of the models and their mathematical expressions were as follows:

$$\mathrm{MSE} = \frac{\sum_{i=1}^{n} \left(y_p - y_e\right)^2}{n}; \quad \text{Mean Square Error} \tag{14}$$

$$\mathrm{PSNR} = 10 \log_{10} \frac{m^2}{\mathrm{MSE}}; \quad \text{Peak Signal - to - Noise Ratio} \tag{15}$$

$$\mathrm{RMSE} = \sqrt{\frac{\sum_{i=1}^{n} \left(y_p - y_e\right)^2}{n}}; \quad \text{Root Mean Square Error} \tag{16}$$

$$\mathrm{NRMSE} = \frac{\mathrm{RMSE}}{\sigma}; \quad \text{Normalized Root Mean Square Error} \tag{17}$$

Table 3 Mechanical test results for (a) Binary blends, (b) Ternary blends (MPa)

Mixture codes	28-days		91-days	
	f_c	f_{ft}	f_c	f_{ft}
(a) Binary blends				
Control	55.93	10.29	60.56	11.15
FA25	52.18	7.49	56.87	8.96
FA30	46.34	7.32	56.09	8.65
FA35	44.05	7.10	47.54	8.64
FA40	41.55	6.80	48.87	8.33
SF5	52.61	7.46	60.33	9.82
SF10	57.63	8.38	62.63	10.12
SF15	56.82	8.70	63.46	10.63
SF20	56.47	9.20	65.16	11.41
(b) Ternary blends (MPa)				
SF5FA25	48.34	8.39	52.97	9.01
SF5FA30	46.24	7.58	51.46	8.77
SF5FA35	40.43	7.69	54.03	8.86
SF5FA40	43.68	7.34	53.74	8.46
SF10FA25	46.19	8.81	56.13	9.50
SF10FA30	44.02	8.52	54.90	8.65
SF10FA35	46.49	7.89	51.93	7.96
SF10FA40	46.18	7.66	54.83	8.16
SF15FA25	48.71	8.85	50.01	8.93
SF15FA30	47.37	8.57	49.65	8.85
SF15FA35	49.78	8.03	52.96	9.10
SF15FA40	49.22	7.54	56.00	9.87
SF20FA25	48.47	8.90	57.15	9.93
SF20FA30	48.66	7.87	52.70	9.28
SF20FA35	38.12	7.07	49.74	7.91
SF20FA40	37.95	7.44	46.35	8.37

$$\mathrm{MAPE} = \frac{1}{n}\left(\sum_{i=1}^{n} \left|\frac{y_p - y_e}{y_p}\right|\right) * 100; \quad \text{Mean Absolute Percentage Error} \tag{18}$$

$$R^2 = 1 - \frac{\sum_{i=1}^{n} \left(y_p - y_e\right)^2}{\sum_{i=1}^{n} \left(y_e - y_p\right)^2}; \quad \text{Coefficient of determination} \tag{19}$$

where y_p and y_e are the predicted and experimental outputs, σ is standard deviation, n is the total number of data, and m is the maximum fluctuation in the input data type. The performance of the devised ML models was assessed for both training and testing data sets. Lower MSE, RMSE, NRMSE, MAPE and higher PSNR values show better prediction performance. The R^2 value denotes how well the predicted data fits the actual data. That is, $R^2 = 1$ means that the data is perfectly fit.

6 Experimental Results

Table 3a and b show the f_c and f_{ft} test results after 28 and 91 curing days for binary and ternary blends of SF and FA. ANOVA was also used to find the influence of experimental variables on the f_c and f_{ft} of SCM. The experimental variables were W/CM, FA, SF and curing time. There were many articles examining the properties of conventional and SCC via ANOVA in the literature (Gupta and Siddique 2020; Mohammed et al. 2019; Tabatabaeian et al. 2017; Tanyildizi and Şahin 2017). The f_c and f_{ft} test results were discussed considering the ANOVA findings in the following sections.

6.1 The Compressive Strength (f_c) Results

The impact of the experimental variables on the results was obtained via ANOVA. Table 4 shows the levels of experimental variables. Observing Table 4, the levels of W/CM, FA, SF, and curing time were 9, 5, 5, and 4. Table 5 indicates the ANOVA results of the f_c of SCMs.

Observing Table 5, the most effective experimental variable for f_c of SCM was the curing time at 86.53%. This may be attributed to the high ratio of pozzolanic material that requires long-term curing to achieve suitable strength (Güneyisi et al. 2015) because 16 of the total mixtures were ternary blends having 30% to 60% pozzolanic material, while eight were binary blends. After the curing time, the most effective experimental variable was the W/CM ratio at 7.07%. Moreover, the error was very low at 2.63%. Some researchers (Güneyisi et al. 2015; Ozbay et al. 2009) used Taguchi and ANOVA methods to evaluate the most important parameter that affects the hardened properties of SCC. According to the research of Ozbay et al. (2009), the most effective experimental variable for compressive strength was the W/CM ratio, while Guneyisi et al. (2015) found that nano-silica had the greatest effect.

The MLR-based model was devised to estimate the f_c of SCMs by using the levels of the experimental variables shown in Table 4. The MLR model equation was given in Eq. (20).

$$\begin{aligned}\mathbf{f_c} = {} & 0.02753 + 0.00352W_1 + 0.00252W_2 \\ & + 0.00145W_3 - 0.00108W_4 + 0.00011W_5 \\ & - 0.00289W_6 - 0.00071W_7 - 0.00028W_8 \\ & - 0.00265W_9 + 0.00801F_1 + 0.000711F_2 \\ & - 0.001547F_3 - 0.003439F_4 - 0.003732F_5 \\ & + 0.000108S_1 - 0.0019S_2 - 0.00107S_3 \\ & + 0.000987S_4 + 0.00187S_5 - 0.015571C_1 \\ & - 0.004816C_2 + 0.007625C_3 + 0.012762C_4\end{aligned} \tag{20}$$

where f_c is compressive strength, $W_1 - W_9$ is the level of W/CM, $F_1 - F_5$ is the fly ash percentage, $S_1 - S_5$ is the silica fume percentage and $C_1 - C_4$ is the level of curing time in Table 4. Figure 6 shows the prediction results of the MLR models.

Observing Fig. 6, the MLR model estimated the f_c of SCMs with 96.79% accuracy. It is obvious that due to the high accuracy, the proposed MLR equation can be used to estimate the f_c of SCMs with high mineral addition. Mohammed et al. (2019) used the ANOVA method to evaluate and optimize eco-friendly SCC. Furthermore, they proposed an MLR model using the experimental variables in the ANOVA. They found that the MLR model estimated the f_c of eco-friendly SCC with 96.95% accuracy. Moreover, the proposed MLR model predicted the fresh properties with 87.23–96.79% accuracy. Raharjo and Subakti (2013) devised an MLR model to estimate the properties of SCC produced from FA, SF, and iron slag as supplementary materials. The proposed model estimated the 28-day f_c of SCC with 75% accuracy.

Table 4 The levels of experimental variables

Variables	Levels	Values
W/CM	9	0.41; 0.42; 0.43; 0.44; 0.45; 0.46; 0.47; 0.48; 0.5
FA (%)	5	0; 25; 30; 35; 40
SF (%)	5	0; 5; 10; 15; 20
Curing Day	4	3; 7; 28; 90

Table 5 The ANOVA results for f_c of SCM

Experimental variables	Degrees of freedom	Sum of squares	Variance	Contribution (%)
W/CM	8	1739.8	217.475	7.07
FA (%)	4	869.7	2176.425	3.54
SF (%)	4	57.4	14.35	0.23
Curing Day	3	21,287	7095.667	86.53
Error	80	646.5	8.081	2.63
Total	99	24,600.5		100

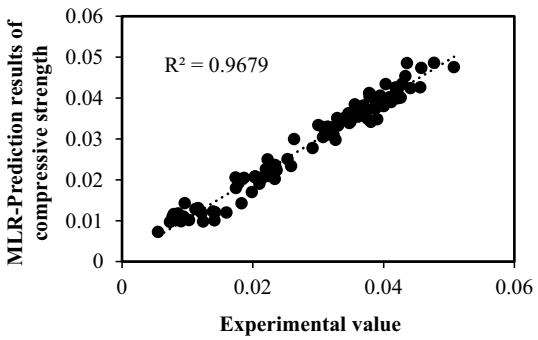


Fig. 6 The prediction results of the MLR and the experimental results for f_c of SCMs

With regard to the f_c test results, the binary blends of SF had the highest values among all SCMs designed. The f_c ranges between 52.61 and 56.47 MPa and 60.33 MPa and 65.16 MPa after 28 and 91 days of curing, respectively, except for SF5. This may be due to the high pozzolanic activity of SF. Also, according to the study of Tikalsky (1992), the silica/calcium ratio in concrete or mortar increases due to the use of SF, and in a hardened state, it depletes $Ca(OH)_2$ and refines the pore size distribution of cement paste leading an improvement in concrete or mortar. On the other hand, at 28 curing days, increasing the SF content of the mixtures did not cause an increasing trend for SF 15 and SF 20 in terms of compressive strength values. The test results were, in fact, very close to each other. This may be attributed to the fact that the workability of the mixtures is adversely affected due to the very small specific surface area of the SF. Observing Table 3, it was found that in the use of binary blend, the f_c of SCMs with FA showed the worst performance at both 28 and 91 curing days. The loss of mechanical strength could be due to replacing a higher percentage (25–40%) of admixture with cement. Because of the reduction of cement components, the early hydration of cement is delayed, and large pore content increases. These pores reduce the strength of the final product. The other researchers (Singh and Goel 2020; Wu et al. 2018) also found similar results. In the literature, it was also noted that calcium in FA forms hydrate assemblages leading to a slow reaction rate, and thus the mechanical strength is reduced (Li et al. 2013). On the other hand, the use of 40% FA caused a slight increase in the compressive strength compared to the use of 30% FA at 90 curing days. This may be attributed to workability, because FA reduces the need for mixing water due to its spherical shape and specific surface. However, the water/binder ratio was kept constant at 0.43 in mixtures with FA. This could cause hydration of more cement grains in the FA40 mixture. In the ternary blends of FA incorporating SF5 and SF20, FA reduced the f_c in general at 28 days, while in the use of FA with SF 10 and SF 15, the amount of FA in general did not cause an important change in the f_c values of SCMs at both 28 and 91 days. It appears that the incorporation of both FA and SF as ternary blends decreased the shortcomings of FA by the beneficial properties of SF. Among all ternary blends, the use of SF 10 or SF15 with FA also caused an improvement in terms of compressive strength with regard to those of the SCMs containing binary blends of FA as the FA content increased. However, the best f_c enhancement was obtained in the ternary blends of SF15FA40 with 18.44% and 14.59% on average for 28 and 91 days, respectively, compared to SCMs containing binary blends of FA. It was obvious from these results that using these two admixtures together in a ternary blend provided a solution to the disadvantages of using FA in a binary blend. Contrary to FA, highly pozzolanic SF consumes CH that was produced at the early hydration of cement. It thereby causes an improvement in the microstructure and refinement of porosity. In this way, SF contributes to the strength enhancement. Similar findings were also obtained by other researchers (Singh and Goel 2020; Turk et al. 2017), who found that the inclusion of mineral admixtures in ternary mixes enhanced the disadvantages of using binary blends of FA.

6.2 Flexural Strength (f_{ft}) Results

Table 3a and b show the experimental results of the f_{ft} test. The influence of experimental variables on the f_{ft} test results was also obtained via the ANOVA approach. The same levels shown in Table 4 were used. Table 6 indicates the ANOVA results of the flexural tensile strength of SCMs.

The most influential parameter was also curing time at 81.32% followed by W/CM with 8.16% and FA with 3.73% for f_{ft}. SF content had the least impact on f_{ft} results with 0.58% due to using a low amount of SF. Moreover, the error was 6.2%.

The MLR-based model was also devised to estimate the f_{ft} of SCMs by using the levels of the experimental variables shown in Table 4. The MLR model equation was given in Eq. (21).

$$\begin{aligned} f_{ft} = {} & 0.005261 - 0.000214W_1 - 0.000063W_2 \\ & - 0.00038W_3 - 0.000619W_4 + 0.000263W_5 \\ & + 0.000031W_6 - 0.000001W_7 + 0.000247W_8 \\ & + 0.000736W_9 + 0.000575F_1 + 0.000301F_2 \\ & - 0.000064F_3 - 0.000315F_4 - 0.000497F_5 \\ & + 0.00023S_1 - 0.000113S_2 - 0.00009S_3 \\ & + 0.000161S_4 - 0.000414S_5 - 0.001982C_1 \\ & - 0.000965C_2 + 0.001051C_3 + 0.001896C_4 \end{aligned} \quad (21)$$

Table 6 The ANOVA results for f_{ft} of SCM

Experimental variables	Degrees of freedom	Sum of squares	Variance	Contribution (%)
W/CM	8	41.743	5.218	8.16
FA (%)	4	19.083	4.77	3.73
SF (%)	4	2.966	0.741	0.58
Curing Day	3	415.88	138.63	81.32
Error	80	31.721	0.40	6.2
Total	99	511.393		100

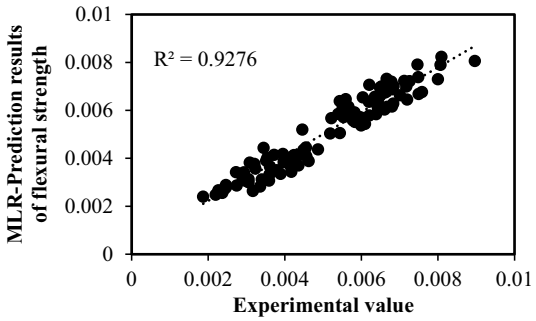


Fig. 7 Prediction results of the MLR and experimental results for f_{ft} of SCMs

where f_{ft} is flexural strength, $W_1 - W_9$ is the level of W/CM, $F_1 - F_5$ is the FA percentage, $S_1 - S_5$ is the SF percentage and $C_1 - C_4$ is the curing time in Table 4. Figure 7 shows the prediction results of the MLR models. Observing Fig. 7, the MLR model estimated the flexural strength of SCMs with 92.76% accuracy. The higher accuracy can show that the proposed MLR equation can be used in the estimation of the f_{ft} of SCMs with high mineral addition.

The f_{ft} value of the control mixture was the highest with 10.29 MPa and 11.15 MPa at 28 and 90 days, respectively, except for SF20. Observing Table 3, similar to f_c values, the f_{ft} of SCMs having binary blends of FA showed worse performance than that of SCMs with the binary blends of SF at both 28 and 91 curing days. In addition, at both 28 and 91 curing days, in the ternary blends, the increase in FA content reduced the f_{ft} value of SCMs except for the mixtures with 15% SF. It can also be stated from this study that, similar to compressive strength, using both FA and SF as ternary blends decreased the shortcomings of FA by the beneficial properties of SF. For example, when the SCMs with binary blends of FA were compared with those of the ternary blends having the same percentage of FA, it was observed that SF contributed to flexural strength enhancement at both 28 and 91 curing days. On the other hand, the ternary blends of FA incorporating SF15 caused the best enhancement with an average of 14.74% and 6.45% at 28 and 91 days, respectively, compared to binary blends having the same percentage of FA.

7 Prediction Results

7.1 ELM Model

In this work, the mechanical properties of SCMs were predicted using an ELM. The architecture of the ELM includes three layers which are input, hidden and output layers. The input layer has six neurons that the input variables: W/CM, curing days, the amounts of cement, FA, SF, and sand. The output layer has two neurons representing the output variables: f_c and f_{ft} of SCMs. A data set containing 100 data samples from experimental works was utilized. The input weights and hidden biases were randomly initialized, and each architecture of the ELM was run ten times. The average of the results was used. The input variables were normalized to the range [0, 1]. The parameters of the ELM were obtained through an empirical approach. The optimal number of hidden neurons was 150. The activation function used for the nonlinear mapping in the hidden layer was sigmoidal as $g(x) = 1/(1 + \exp(-x))$. The testing-training data sets of the ELM model were randomly generated from the overall data set, and 90% of the data were employed for training while the rest were used for testing. The prediction results for f_c and f_{ft} of SCMs were given in Figs. 8 and 9.

Observing Figs. 8 and 9, the R^2 coefficients for both the f_c and f_{ft} of SCMs were 0.9802. The ELM model carried out very good predictions due to having a correlation coefficient as high as $R^2 = 1$ for each strength metric. The accuracy were highly comparable with those of the training process for both strength metrics, which means that the ELM model demonstrated superior generalized performance without overfitting. Besides, the R^2 values for f_c and f_{ft} of SCMs were the same, which indicates that the performance of the ELM for f_c and f_{ft} of SCMs was similar. The performance results of the devised ELM were given in Table 7. The values of RMSE and MAPE of the f_c predicted by the ELM model were 1.9131 and 5.1182 and these values were 0.5654 and 9.2378 for f_{ft}, respectively. Tanyildizi et al. (2022) also predicted the f_c of concrete with microencapsulated phase-change materials using a hybrid ELM-autoencoder model and they found the *R*-squared, RMSE and MAE values as 0.968, 3.211, and 2.625, respectively. Peng and Unluer (2022) estimated the f_c

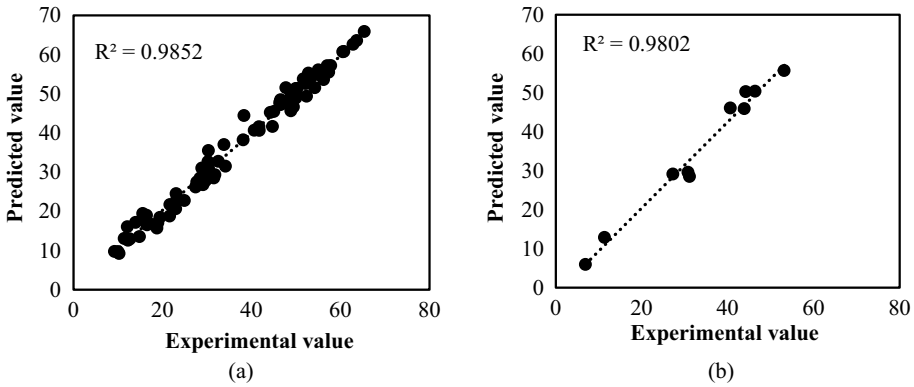


Fig. 8 The linear relationship between predicted and measured f_c of SCMs based on ELM for **a** training and **b** testing

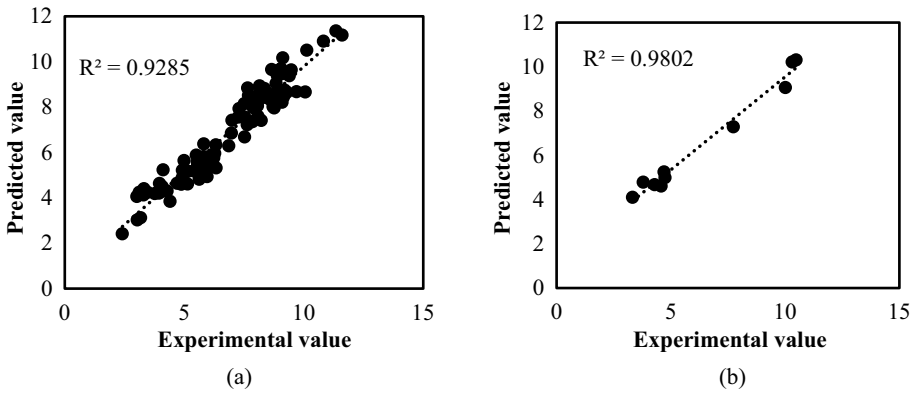


Fig. 9 The linear relationship between predicted and measured f_{ft} of SCMs based on ELM for **a** training and **b** testing

Table 7 The performance results of the ELM for f_c and f_{ft} of SCMs

	f_c		f_{ft}	
	Training	Testing	Training	Testing
MSE	10.6742	3.6601	0.3437	0.3197
PSNR	37.8474	42.4959	52.7689	53.0833
RMSE	3.2671	1.9131	0.5863	0.5654
NRMSE	0.0707	0.0341	0.0637	0.0790
MAPE	9.1881	5.1182	7.7363	9.2378

of geopolymer concrete via a back-propagation neural network (BPNN), SVM, and ELM. The highest *R*-squared value was obtained in the BPNN, at 0.8221, while it was 0.7032 for the ELM, but SVM revealed more stable prediction accuracy. Hence, the proposed ELM model predicted the compressive and flexural strength better than the literature.

7.2 SVR Model

In this work, the accuracy of the SVR was also evaluated with respect to the mechanical properties of SCMs. The testing and training sets were the same as the ELM. The radial basis kernel function was used in this model. Regardless of the input and output variables, there are model parameters such as C, ε, and γ in the SVR model. In order to predict the output variables (f_c and f_{ft}) using the input variables (W/CM, curing days, the amounts of cement, FA, SF, and sand), the values of the model parameters are specified. The optimal values of the model parameters had an important effect on the accuracy of the SVR model. The values of C, ε, and γ were selected as 0.001024, 4.4102, and 0.0011, respectively, via trial and error. The prediction results of the SVR model for f_c and f_{ft} of SCMs were given in Figs. 10 and 11.

The SVR estimated the f_c and f_{ft} of SCMs with 63.3% and 84.26% accuracy, respectively. It is obvious that the SVR model predicted the f_{ft} with a better coefficient of determination than that of f_c. Referring to Table 8, the lower MSE, RMSE, MAPE and NRMSE as well as the higher PSNR were obtained for the testing data set of the SVR model for flexural strength of SCMs as expected. This indicates that the SVR model can be reliable for the forecasting of flexural strength of SCMs with high mineral addition, while some alternative ML approaches are necessary for compressive strength. The RMSE and MAPE values were 8.9838 and 46.8222, respectively, for the prediction of f_c. These values were 1.1318 and 15.6679 for f_{ft}. In Kina et al. (2022a), the strengths of SCC with fiber hybridization were also predicted using SVR and deep-learning models, and it was found that the f_c, splitting tensile and f_{ft} of SCC were

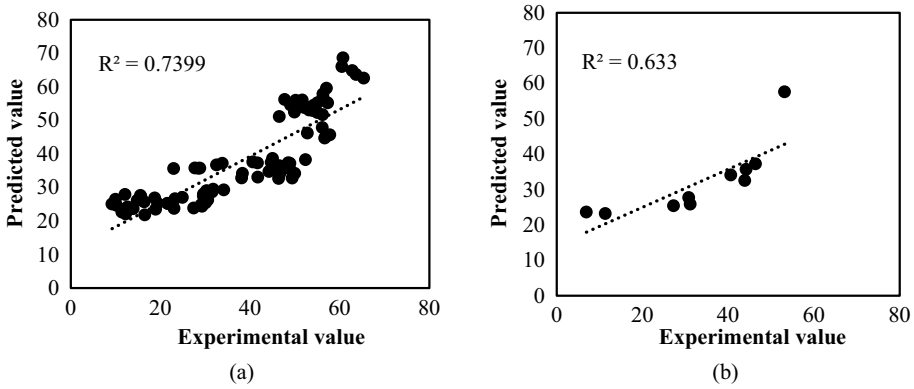


Fig. 10 The linear relationship between predicted and measured f_c of SCMs based on the SVR for **a** training and **b** testing

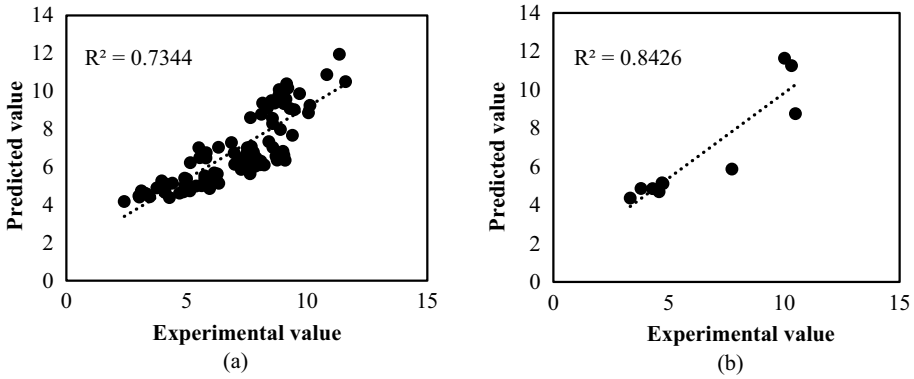


Fig. 11 The linear relationship between predicted and measured f_{ft} of SCMs based on SVR for **a** training and **b** testing

Table 8 The performance results of the SVR for f_c and f_{ft} of SCMs

	f_c		f_{ft}	
	Training	Testing	Training	Testing
MSE	65.1044	80.7083	1.2905	1.2811
PSNR	29.9947	29.0616	47.0233	47.0551
RMSE	8.0687	8.9838	1.1360	1.1318
NRMSE	0.1438	0.1943	0.1235	0.1581
MAPE	26.4102	46.8222	16.0421	15.6679

estimated via deep learning model with99.27%, 98.59%, and 99.15% accuracy, respectively. On the other hand, Azimi-Pour et al. (2020) selected SVR to predict the properties of SCC having high FA content. In their models, they used 337 samples for the compressive strength from the literature. They estimated the f_c of SCC with 93.88% accuracy. Saha et al. (2020) used SVR to estimate the f_c and fresh properties of SCC using 115 test samples. They found the results of compressive strength and fresh concrete properties with an accuracy of 95.5% and 91–95.8%, respectively. In conclusion, the proposed SVR model was found to estimate the compressive and flexural strength with lower accuracy than that in the literature.

7.3 ANN Model

In this study, the f_c and f_{ft} of SCMs were also estimated using an ANN model. Similar to the ELM and SVR models, 90% and 10% of all data were used for training–testing, respectively. The determination of the architecture of a neural network is important because it directly influences the generalization capability and computational complexity (Kişi and Uncuoğlu 2005). A multilayer feed-forward network model with one hidden layer can approximate a complex nonlinear function provided that a sufficiently large number of hidden-layer neurons are present (Saridemir 2009). For this reason, the multilayer feed-forward network model with one hidden layer was used. The determination of the optimal number of hidden layer neurons has also a significant effect on the accuracy of the ANN. Due to the lack of theory related to finding the optimal value, two neurons were tried at first, and then it was increased slightly by adding one neuron. The performance of the model was monitored for each hidden-neuron number. This process continued until the error was acceptably small, and the best performance was obtained from the ANN model with 20 hidden-layer neurons. The gradient descent algorithm with moment back-propagation was used for training because, among other functions, it gave the most appropriate training function. The prediction

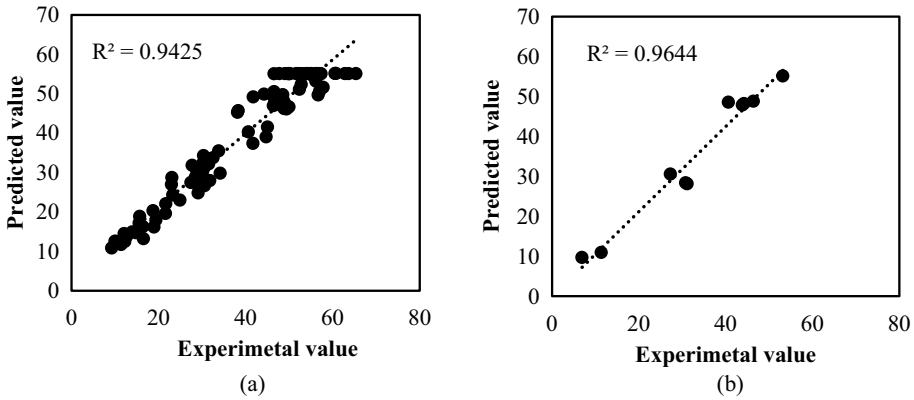


Fig. 12 The linear relationship between predicted and measured f_c of SCMs based on ANN for **a** training and **b** testing

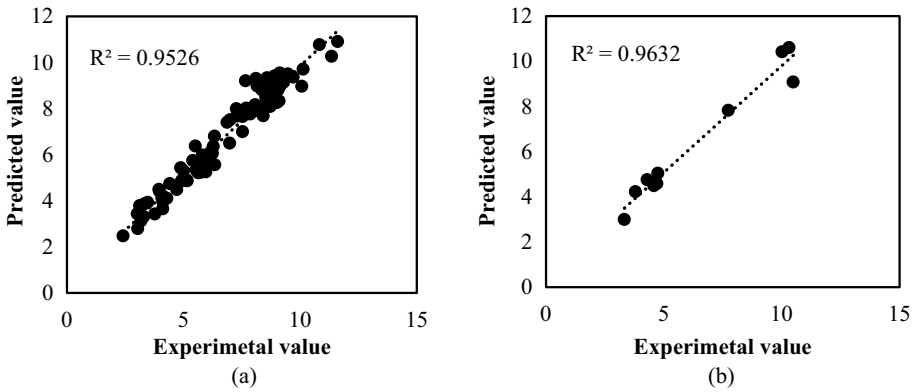


Fig. 13 The linear relationship between predicted and measured f_{ft} of SCMs based on ANN for **a** training and **b** testing

Table 9 The performance results of the ANN for f_c and f_{ft} of SCMs

	f_c		f_{ft}	
	Training	Testing	Training	Testing
MSE	14.2779	13.8229	0.2280	0.2841
PSNR	36.5842	36.7248	54.5507	53.5953
RMSE	3.7786	3.7179	0.4775	0.5331
NRMSE	0.0673	0.0804	0.0519	0.0744
MAPE	8.3398	11.9780	5.7372	6.3898

results of the ANN model for f_c and f_{ft} of SCMs were given in Figs. 12 and 13.

Observing Figs. 12 and 13, the ANN model estimated the f_c and f_{ft} of SCMs with 96.44% and 96.32% accuracy, respectively. Although high values of the coefficient of determination were obtained for both f_c and f_{ft} of SCMs, the performance of the ANN model for f_c of SCMs was better than that of the ANN model for f_{ft} of SCMs. This was also proven by the performance evaluation results due to lower MSE, RMSE, MAPE and NRMSE as well as higher PSNR. Observing Table 9, the RMSE and MAPE values were 3.7179 and 11.9780 for the prediction of f_c using the ANN model, respectively, and these values were 0.5331 and 6.3898 for f_{ft}. In Meesaraganda et al. (2019), the f_c of fiber-reinforced SCC was also estimated via an ANN by using 99 test samples with a 6.2% error. Taheri et al. (2019) devised the ANN, MLR models, and gene-expression programming models for the f_c of SCC. In their experiments, 156 samples with rice husk ash were used, and the best results were obtained from the gene-expression programming. In Kandiri et al. (2021), a genetic algorithm (GA), salp swarm algorithm (SSA), and grasshopper optimization algorithm (GOA) were employed to modify an ANN to predict the f_c of concrete with recycled aggregate. A data set containing 234 patterns was used from the literature, and it was found that the ANN hybridized with SSA had the lowest RMSE value with 2.734.

7.4 DT Model

In this study, a DT was also developed for the prediction of the f_c and f_{ft} of SCMs. As in the case of other ML algorithms, 90% and 10% of all data were used for training–testing, respectively, and also the same input and output parameters were used. The DT model was devised by splitting the data set into branch-like segments. Referring to Fig. 14, the developed tree model had 14 nodes and 15 leaves. It was created automatically as a result of the development of ML techniques based on the data set collected from the

experimental process. The prediction results of the DT model for f_c and f_{ft} of SCMs were given in Figs. 15 and 16.

According to the results obtained from the DT, the R^2 values were 0.9676 and 0.8581 for f_c and f_{ft} of SCMs, respectively. The f_c of SCMs with high mineral addition was predicted by the DT with higher accuracy than the f_{ft} of SCMs. The performance results of the devised model were given in Table 10. As expected, for the f_c of SCMs,

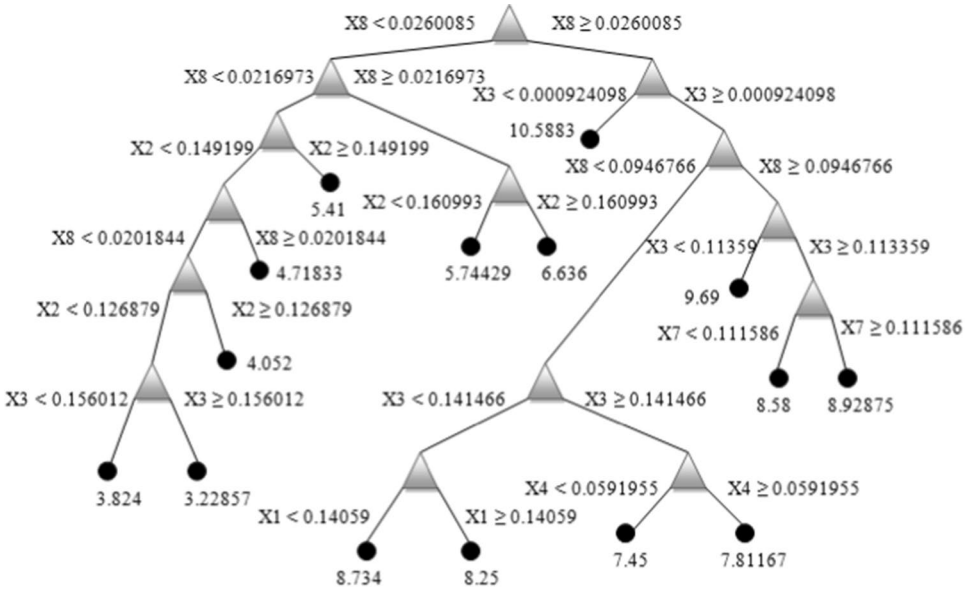


Fig. 14 The visualization of the training process of DT

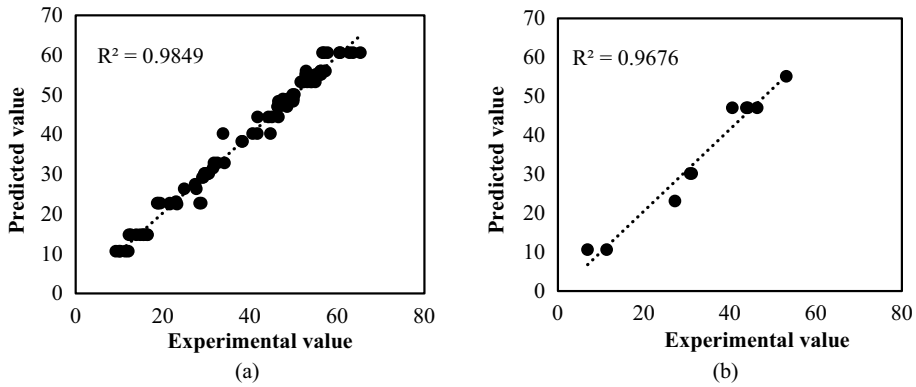


Fig. 15 The linear relationship between predicted and measured f_c of SCMs based on DT for **a** training and **b** testing

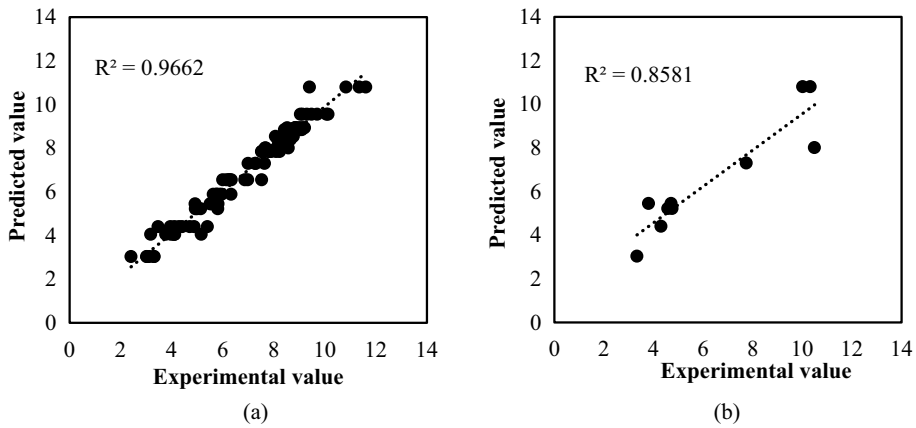


Fig. 16 The linear relationship between predicted and measured f_{ft} of SCMs based on DT for **a** training and **b** testing

Table 10 The performance results of the DT for f_c and f_{ft} of SCMs

	f_c		f_{ft}	
	Training	Testing	Training	Testing
MSE	3.7389	1.1185	0.1625	9.5625
PSNR	42.4034	47.6445	56.0209	38.3251
RMSE	1.9336	1.0576	0.4032	3.0923
NRMSE	0.0344	0.0669	0.0438	0.1477
MAPE	4.3914	11.4690	4.9681	13.5948

lower MSE, RMSE, MAPE and NRMSE as well as higher PSNR were found compared to the f_{ft} of SCMs. The values of RMSE and MAPE were found as 1.0576 and 11.4690 for the prediction of f_c using DT model, respectively, and these values were 3.0923 and 13.5948 for f_{ft}. In Latif (2021),SVR and boosted decision tree regression (BDTR) models were devised to estimate the *fc* of environmentally friendly concrete, and it was noted that the BDTR had better performance compared to the SVR, with a *R*-squared value of 0.86 . Ma et al. (2021) compared the accuracy of SVR, DT, and RF models for the prediction of the f_c of cement-based materials with mining waste. They found that the RF model showed the best performance due to having the highest R and lowest RMSE values with 0.9731 and 0.2286, respectively. Ahmad et al. (2022) also developed DT, bagging regressor (BR), and AdaBoost regressor (AR) to predict the f_c of geopolymer concrete with FA, and they indicated that the BR model was more effective, with an *R*-squared value of 0.97. It was concluded that the predictions obtained from the proposed DT model for compressive and flexural strengths were consistent with the literature findings.

7.5 Comparison of the ELM Model with Other ML Models

A Taylor diagram was constructed to reveal how closely the developed ML algorithms matched the actual and corresponding predicted values. This is the most commonly recommended diagram to compare the realistic characteristics and accuracy of the models due to its ability to quantify and combine multiple statistical metrics by measuring the difference between the predicted and measured values in one diagram (Elkiran et al. 2019; Zhou et al. 2017). Observing Fig. 17, the real value is referred to as a reference point on the line $R=1$ and in the center of the RMSE (Taylor 2001). For both compressive and flexural strength predictions, the ELM model was closer to the real measured values compared to the other three developed ML models with relatively low RMSE values and high correlation coefficients. Referring to Table 11, the RMSE values of the ELM model were 1.9131 and 0.5654 for compressive and flexural strengths, respectively. Therefore, it was found that the ELM demonstrated the best performance in terms of modeling and prediction of the f_c and f_{ft} of SCMs with high mineral addition with regard to SVR, ANN, and DT models. Among the other three ML models, the performance of the ANN model was also promising, with RMSE values of 3.7179 and 0.5331 for compressive and flexural strengths, respectively, and higher correlation coefficients. Of the poorer-performing models, SVR had a larger standard deviation and a lower correlation coefficient, resulting in a higher RMSE value with 8.9838 and 1.1318 for the prediction of f_c and f_{ft}, respectively.

It is crucial to state that, except for the SVR model devised for the prediction of compressive strengths, there is

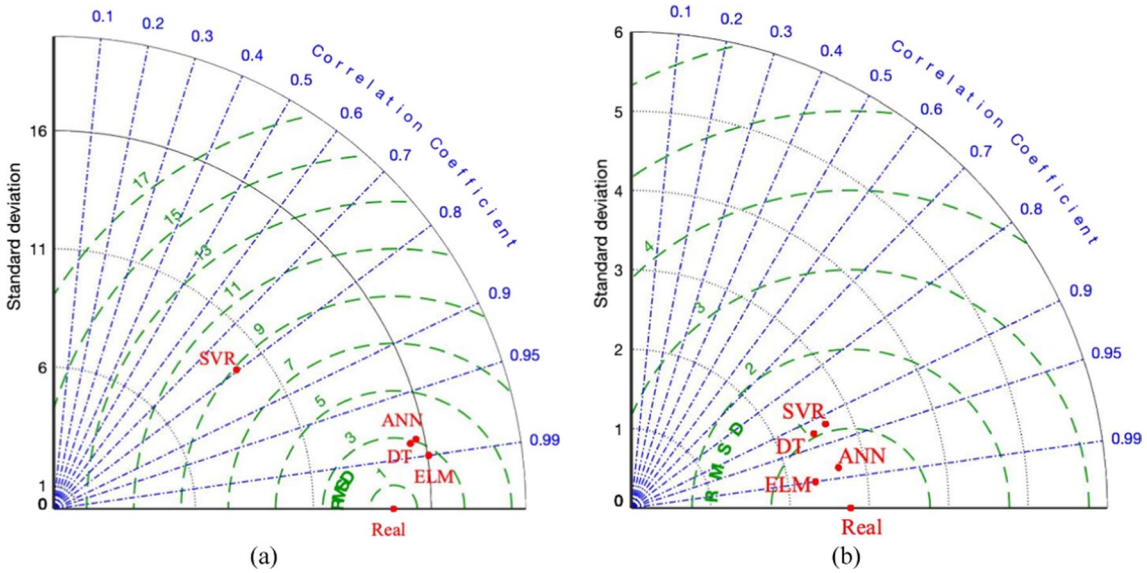


Fig. 17 Taylor diagram of ML models for **a** f_c, **b** f_{ft} of SCMs with high mineral addition

Table 11 Predictive performance of different ML models on the test set

Performance metrics	f_c				f_{ft}			
	ELM	SVR	ANN	DT	ELM	SVR	ANN	DT
MSE	3.6601	80.7083	13.8229	9.5625	0.3197	1.2811	0.2841	1.1185
PSNR	42.4959	29.0616	36.7248	38.3251	53.0833	47.0551	53.5953	47.6445
R-squared	0.9802	0.6330	0.9644	0.9676	0.9802	0.8426	0.9632	0.8581
RMSE	1.9131	8.9838	3.7179	3.0923	0.5654	1.1318	0.5331	1.0576
NRMSE	0.0341	0.1943	0.0804	0.0669	0.0790	0.1581	0.0744	0.1477
MAPE	5.1182	46.8222	11.9780	11.4690	9.2378	15.6679	6.3898	13.5948

no exceptional model that performed separately from other ML models, as seen in Fig. 17. This means that, in this study, there is performance uniformity of the ML models. However, the ELM model yielded superior predictions compared to those of the SVR, ANN, and DT models in this study, so it is suggested to use the ELM model for the predictions of the f_c and f_{ft} of SCMs with high mineral addition.

8 Summary and Conclusions

In this work, an experimental study was carried out to investigate the effects of a high volume of FA and SF as binary and ternary blends in SCMs for environmental awareness. A total of 300 specimens were designed, and the f_c and f_{ft} tests were performed. To avoid expensive and time-consuming lab tests, this paper presented four ML approaches including ELM, SVR, ANN, and DT models, and compared the results obtained from these prediction methods to reveal the utility of the ELM model in the field of civil engineering. The contributions of the experimental parameters were also examined by ANOVA, and MLR equations were proposed based on the input parameters defined in each ML model.

The experimental results showed that the SCMs having binary blends of SF in general showed the best performance among all SCMs with regard to f_c, while the inclusion of FA into mixtures reduced the f_c at 28 and 91 curing days. However, the use of SF10 or SF15 with FA as ternary blends leads to an improvement in f_c compared to SCMs having binary blends of FA as FA content increased. As for the f_{ft} test results, the values of the control mixture were the highest at both 28 and 91 days among all SCMs in general. Besides, the increase in FA content generally induced a decrease in the f_{ft} of SCMs with binary and ternary blends at 28 and 91 days. However, in the use of SF with FA as ternary blends, SF contributed to f_{ft} enhancement after both 28 and 90 curing days with regard to SCMs with binary blends of FA. ANOVA showed that the curing time had the highest impact on both f_c and f_{ft} test results, with 86.53% and 81.32%, respectively.

The ELM, SVR, ANN, and DT models predicted the compressive strength values with 98.02%, 63.3%, 96.44%, and 96.76% accuracy, respectively, while the same models for flexural strength resulted in 98.02%, 84.26%, 96.32%, and 85.51% accuracy, respectively. It is clear that the ML approaches developed in this study gave strong relations between predicted and actual results. The higher accuracy percentages show the significance of these ML models in the field of civil engineering, especially for the prediction of the mechanical properties of concrete. However, based on the performance metrics determined here, it was found that the ELM model demonstrated superior generalized performance, indicating the highest accuracy compared to other ML models. Consequently, the ELM model can be used to predict the mechanical properties of SCMs, SCC, conventional mortar or concrete, geopolymer mortar or concrete.

Author contributions All authors contributed to the study conception and design. Material preparation, data collection and analysis were performed by KT, CK and HT. All authors read and approved the final manuscript.

Data availability All data and materials support the published claims and comply with field standards.

Code availability Software application or custom code support the published claims and comply with field standards.

Declarations

Conflict of interest The authors declare that they have no conflict of interest.

References

Ahmad A, Farooq F, Niewiadomski P, Ostrowski K, Akbar A, Aslam F, Alyousef R (2021a) Prediction of compressive strength of fly ash based concrete using individual and ensemble algorithm. Materials 14(4):1–21

Ahmad A, Farooq F, Ostrowski KA, Śliwa-Wieczorek K, Czarnecki S (2021b) Application of novel machine learning techniques for predicting the surface chloride concentration in concrete containing waste material. Materials 14(9):2297

Ahmad A, Ahmad W, Aslam F, Joyklad P (2022) Compressive strength prediction of fly ash-based geopolymer concrete via advanced machine learning techniques. Case Stud Constr Mater 16:e00840

Alçin ÖF, Şengür A, Ince MC (2015) Forward-backward pursuit based sparse extreme learning machine. J Fac Eng Arch Gazi Univ 30(1):111–117

Alcin OF, Sengur A, Ghofrani S, Ince MC (2014) GA-SELM: greedy algorithms for sparse extreme learning machine. Meas J Int Meas Confed 55:126–132

Al-Shamiri AK, Kim JH, Yuan TF, Yoon YS (2019) Modeling the compressive strength of high-strength concrete: an extreme learning approach. Constr Build Mater 208:204–219

Anjos MAS, Camões A, Campos P, Azeredo GA, Ferreira RLS (2020) Effect of high volume fly ash and metakaolin with and without hydrated lime on the properties of self-compacting concrete. J Build Eng 27:100985

Aprianti E, Shafigh P, Zawawi R, Abu Hassan ZF (2016) Introducing an effective curing method for mortar containing high volume cementitious materials. Constr Build Mater 107:365–377

Asteris PG, Mokos VG (2020) Concrete compressive strength using artificial neural networks. Neural Comput Appl 32(15):11807–11826

ASTM C39/C39M-20 (2020) Standard test method for compressive strength of cylindrical concrete specimens

ASTM-C09 (2000) Standard test method for flexural strength of concrete (Using simple beam with center-point loading)

Atis CD, Tanyildizi H, Karahan O (2009) Statistical analysis for strength properties of polypropylene-fibre- reinforced fly ash concrete. Mag Concr Res 61(7):557–566

Azimi-Pour M, Eskandari-Naddaf H, Pakzad A (2020) Linear and non-linear SVM prediction for fresh properties and compressive strength of high volume fly ash self-compacting concrete. Constr Build Mater 230:117021

Bagheri A, Zanganeh H, Alizadeh H, Shakerinia M, Marian MAS (2013) Comparing the performance of fine fly ash and silica fume in enhancing the properties of concretes containing fly ash. Constr Build Mater 47:1402–1408

Barcelo L, Kline J, Walenta G, Gartner E (2014) Cement and carbon emissions. Mater Struct Mater Constr 47(6):1055–1065

Ben Chaabene W, Flah M, Nehdi ML (2020) Machine learning prediction of mechanical properties of concrete: critical review. Constr Build Mater 260:119889

Benhelal E, Zahedi G, Shamsaei E, Bahadori A (2013) Global strategies and potentials to curb CO_2 emissions in cement industry. J Clean Prod 51:142–161

Benli A, Turk K, Kina C (2018) Influence of silica fume and class F fly ash on mechanical and rheological properties and freeze-thaw durability of self-compacting mortars. J Cold Reg Eng 32(3):04018009

Bin HG (2003) Learning capability and storage capacity of two-hidden-layer feedforward networks. IEEE Trans Neural Netw 14(2):274–281

Bin HG, Zhu QY, Siew CK (2006) Extreme learning machine: theory and applications. Neurocomputing 70(1–3):489–501

Chajec A (2021) Granite powder vs. fly ash for the sustainable production of air-cured cementitious mortars. Materials 14(5):1–26

Chatterjee A, Das D (2013) Assessing flow response of self-compacting mortar by Taguchi method and ANOVA interaction. Mater Res 16(5):1084–1091

Cherkassky V, Mulier F (2006) Learning from data: concepts, theory, and methods, 2nd edn. Wiley, New Jersey

Cotsovos DM, Pavlović MN (2008) Numerical investigation of concrete subjected to compressive impact loading. Part 2: parametric investigation of factors affecting behaviour at high loading rates. Comput Struct 86(1–2):164–180

Cristianini N, Shawe-Taylor J (2000) An introduction to support vector machines and other kernel-based learning methods

Czarnecki S, Shariq M, Nikoo M, Sadowski Ł (2021) An intelligent model for the prediction of the compressive strength of cementitious composites with ground granulated blast furnace slag based on ultrasonic pulse velocity measurements. Meas J Int Meas Confed 172:108951

Das D, Chatterjee A (2014) Taguchi and ANOVA approach for optimization of flow characteristics of self-compacting concrete. Emerg Mater Res 3(1):37–45

Diniz HAA, dos Anjos MAS, Rocha AKA, Ferreira RLS (2022) Effects of the use of agricultural ashes, metakaolin and hydrated-lime on the behavior of self-compacting concretes. Constr Build Mater 319:126087

Dou J, Yunus AP, Tien Bui D, Merghadi A, Sahana M, Zhu Z, Chen CW, Khosravi K, Yang Y, Pham BT (2019) Assessment of advanced random forest and decision tree algorithms for modeling rainfall-induced landslide susceptibility in the Izu-Oshima Volcanic Island, Japan. Sci Total Environ 662:332–346

EFNARC (2002) Specification and guidelines for self-compacting concrete. Report from EFNARC

Elkiran G, Nourani V, Abba SI (2019) Multi-step ahead modelling of river water quality parameters using ensemble artificial intelligence-based approach. J Hydrol 577:123962

Falmata AM, Sulaiman A, Mohamed RN, Shettima AU (2020) Mechanical properties of self-compacting high-performance concrete with fly ash and silica fume. SN Appl Sci 2(33):1–11

Farooq F, Akbar A, Khushnood RA, Muhammad WLB, Rehman SKU, Javed MF (2020) Experimental investigation of hybrid carbon nanotubes and graphite nanoplatelets on rheology, shrinkage, mechanical, and microstructure of SCCM. Materials 13(1):230

Farooq F, Ahmed W, Akbar A, Aslam F, Alyousef R (2021) Predictive modeling for sustainable high-performance concrete from industrial wastes: a comparison and optimization of models using ensemble learners. J Clean Prod 292:126032

Feng DC, Liu ZT, Wang XD, Chen Y, Chang JQ, Wei DF, Jiang ZM (2020) Machine learning-based compressive strength prediction for concrete: an adaptive boosting approach. Constr Build Mater 230:117000

Gao W, Karbasi M, Derakhsh AM, Jalili A (2019) Development of a novel soft-computing framework for the simulation aims: a case study. Eng Comput 35(1):315–322

Golafshani EM, Behnood A, Arashpour M (2020) Predicting the compressive strength of normal and high-performance concretes using ANN and ANFIS hybridized with grey wolf optimizer. Constr Build Mater 232:117266

Güçlüer K, Özbeyaz A, Göymen S, Günaydın O (2021) A comparative investigation using machine learning methods for concrete compressive strength estimation. Mater Today Commun 27:102278

Güneyisi E, Gesoğlu M (2008) Properties of self-compacting mortars with binary and ternary cementitious blends of fly ash and metakaolin. Mater Struct Mater Constr 41(9):1519–1531

Güneyisi E, Gesoglu M, Al-Goody A, Ipek S (2015) Fresh and rheological behavior of nano-silica and fly ash blended self-compacting concrete. Constr Build Mater 95:29–44

Gupta T, Patel KA, Siddique S, Sharma RK, Chaudhary S (2019) Prediction of mechanical properties of rubberised concrete exposed to elevated temperature using ANN. Meas J Int Meas Confed 147:106870

Gupta N, Siddique R (2020) Durability characteristics of self-compacting concrete made with copper slag. Constr Build Mater 247:118580

Jahangir H, Rezazadeh Eidgahee D (2021) A new and robust hybrid artificial bee colony algorithm – ANN model for FRP-concrete bond strength evaluation. Compos Struct 257:113160

Jalal M, Pouladkhan A, Harandi OF, Jafari D (2015) Comparative study on effects of Class F fly ash, nano silica and silica fume on properties of high performance self compacting concrete. Constr Build Mater 94:90–104

Jueyendah S, Lezgy-Nazargah M, Eskandari-Naddaf H, Emamian SA (2021) Predicting the mechanical properties of cement mortar using the support vector machine approach. Constr Build Mater 291:123396

Kajaste R, Hurme M (2016) Cement industry greenhouse gas emissions—management options and abatement cost. J Clean Prod 112:4041–4052

Kandiri A, Sartipi F, Kioumarsi M (2021) Predicting compressive strength of concrete containing recycled aggregate using modified ann with different optimization algorithms. Appl Sci (switzerland) 11(2):1–19

Karahan O, Tanyildizi H, Atis CD (2008) An artificial neural network approach for prediction of long-term strength properties of steel fiber reinforced concrete containing fly ash. J Zhejiang Univ Sci A 9(11):1514–1523

Karbassi A, Mohebi B, Rezaee S, Lestuzzi P (2014) Damage prediction for regular reinforced concrete buildings using the decision tree algorithm. Comput Struct 130:46–56

Karimipour A, Bagherzadeh SA, Taghipour A, Abdollahi A, Safaei MR (2019) A novel nonlinear regression model of SVR as a substitute for ANN to predict conductivity of MWCNT-CuO/water hybrid nanofluid based on empirical data. Phys A 521:89–97

Kina C, Turk K, Atalay E, Donmez I, Tanyildizi H (2021) Comparison of extreme learning machine and deep learning model in the estimation of the fresh properties of hybrid fiber-reinforced SCC. Neural Comput Appl 33:11641–11659

Kina C, Turk K, Tanyildizi H (2022a) Estimation of strengths of hybrid FR-SCC by using deep-learning and support vector regression models. Struct Concr 23:3313–3330

Kina C, Turk K, Tanyildizi H (2022b) Deep learning and machine learning-based prediction of capillary water absorption of hybrid fiber reinforced self-compacting concrete. Struct Concr 23:3331–3358

Kişi Ö, Uncuoğlu E (2005) Comparison of three back-propagation training algorithms for two case studies. Indian J Eng Mater Sci 12(5):434–442

Lan Y, Soh YC, Bin HG (2010) Constructive hidden nodes selection of extreme learning machine for regression. Neurocomputing 73(16–18):3191–3199

Larissa LC, Marcos MA, Maria MV, de Souza SLN, de Farias EC (2020) Effect of high temperatures on self-compacting concrete with high levels of sugarcane bagasse ash and metakaolin. Constr Build Mater 248:118715

Latif SD (2021) Developing a boosted decision tree regression prediction model as a sustainable tool for compressive strength of environmentally friendly concrete. Environ Sci Pollut Res 28(46):65935–65944

Li X, Ma X, Zhang S, Zheng E (2013) Mechanical properties and microstructure of class C fly ash-based geopolymer paste and mortar. Materials 6(4):1485–1495

Lv Y, Liu J, Yang T, Zeng D (2013) A novel least squares support vector machine ensemble model for NO_x emission prediction of a coal-fired boiler. Energy 55:319–329

Ma H, Liu J, Zhang J, Huang J (2021) Estimating the compressive strength of cement-based materials with mining waste using support vector machine, decision tree, and random forest models. Adv Civ Eng 2021:1–10

Madandoust R, Mousavi SY (2012) Fresh and hardened properties of self-compacting concrete containing metakaolin. Constr Build Mater 35:752–760

Meesaraganda LVP, Saha P, Tarafder N (2019) Artificial neural network for strength prediction of fibers' self-compacting concrete. Adv Intell Syst Comput 816:15–24

Megat Johari MA, Brooks JJ, Kabir S, Rivard P (2011) Influence of supplementary cementitious materials on engineering properties of high strength concrete. Constr Build Mater 25(5):2639–2648

Mohammed MK, Al-Hadithi AI, Mohammed MH (2019) Production and optimization of eco-efficient self compacting concrete SCC with limestone and PET. Constr Build Mater 197:734–746

Moradi MJ, Khaleghi M, Salimi J, Farhangi V, Ramezanianpour AM (2021) Predicting the compressive strength of concrete containing metakaolin with different properties using ANN. Meas J Int Meas Confed 183:109790

Naderpour H, Rafiean AH, Fakharian P (2018) Compressive strength prediction of environmentally friendly concrete using artificial neural networks. J Build Eng 16:213–219

Ozbay E, Oztas A, Baykasoglu A, Ozbebek H (2009) Investigating mix proportions of high strength self compacting concrete by using Taguchi method. Constr Build Mater 23(2):694–702

Özcan F, Atiş CD, Karahan O, Uncuoğlu E, Tanyildizi H (2009) Comparison of artificial neural network and fuzzy logic models for prediction of long-term compressive strength of silica fume concrete. Adv Eng Softw 40(9):856–863

Peng Y, Unluer C (2022) Analyzing the mechanical performance of fly ash-based geopolymer concrete with different machine learning techniques. Constr Build Mater 316:125785

Raharjo D, Subakti A (2013) Mixed concrete optimization using fly ash, silica fume and iron slag on the SCC's compressive strength. Procedia Eng 54:827–839

Saha P, Debnath P, Thomas P (2020) Prediction of fresh and hardened properties of self-compacting concrete using support vector regression approach. Neural Comput Appl 32(12):7995–8010

Salami BA, Rahman SM, Oyehan TA, Maslehuddin M, Al Dulaijan SU (2020) Ensemble machine learning model for corrosion initiation time estimation of embedded steel reinforced self-compacting concrete. Meas J Int Meas Confed 165:108141

Saridemir M (2009) Prediction of compressive strength of concretes containing metakaolin and silica fume by artificial neural networks. Adv Eng Softw 40(5):350–355

Shahin MA, Jaksa MB, Maier HR (2009) Recent advances and future challenges for artificial neural systems in geotechnical engineering applications. Adv Artif Neural Syst 2009:1–9

Siddique R (2011) Properties of self-compacting concrete containing class F fly ash. Mater Des 32(3):1501–1507

Singh R, Goel S (2020) Experimental investigation on mechanical properties of binary and ternary blended pervious concrete. Front Struct Civ Eng 14(1):229–240

Su M, Zhong Q, Peng H, Li S (2021) Selected machine learning approaches for predicting the interfacial bond strength between FRPs and concrete. Constr Build Mater 270:121456

Sultana N, Zakir Hossain SM, Alam MS, Islam MS, Al AMA (2020) Soft computing approaches for comparative prediction of the mechanical properties of jute fiber reinforced concrete. Adv Eng Softw 149:102887

Tabatabaeian M, Khaloo A, Joshaghani A, Hajibandeh E (2017) Experimental investigation on effects of hybrid fibers on rheological, mechanical, and durability properties of high-strength SCC. Constr Build Mater 147:497–509

Taheri Amiri MJ, Ashrafian A, Haghighi FR, Javaheri Barforooshi M (2019) Prediction of the compressive strength of self-compacting concrete containing rice husk ash using data driven models. Modares Civ Eng J 19(1):196–206

Tanyildizi H (2021) Predicting the geopolymerization process of fly ash-based geopolymer using deep long short-term memory and machine learning. Cement Concr Compos 123:104177

Tanyildizi H, Şahin M (2017) Taguchi optimization approach for the polypropylene fiber reinforced concrete strengthening with polymer after high temperature. Struct Multidiscip Optim 55(2):529–534

Tanyildizi H, Şengür A, Akbulut Y, Şahin M (2020) Deep learning model for estimating the mechanical properties of concrete containing silica fume exposed to high temperatures. Front Struct Civ Eng 14:1316–1330

Tanyildizi H, Marani A, Türk K, Nehdi ML (2022) Hybrid deep learning model for concrete incorporating microencapsulated phase change materials. Constr Build Mater 319:126146

Tanyildizi H, Coşkun A, Somunkiran I (2008) An experimental investigation of bond and compressive strength of concrete with mineral admixtures at high temperatures. Arab J Sci Eng 33(2B):443–449

Tanyildizi H (2018) Long-term performance of the healed mortar with polymer containing phosphazene after exposed to sulfate attack. Constr Build Mater 167:473–481

Tanyildizi H (2018) Prediction of the strength properties of carbon fiber-reinforced lightweight concrete exposed to the high temperature using artificial neural network and support vector machine. Adv Civ Eng 2018:1–10

Taylor KE (2001) Summarizing multiple aspects of model performance in a single diagram. J Geophys Res Atmos 106(D7):7183–7192

Tikalsky PJ, Carrasquillo RL (1992) Influence of fly ash on the sulfate resistance of concrete. ACI Mater J 89(1):69–75

Turk K (2012) Viscosity and hardened properties of self-compacting mortars with binary and ternary cementitious blends of fly ash and silica fume. Constr Build Mater 37:326–334

Turk K, Kina C (2018) Freeze-thaw resistance and sorptivity of self-compacting mortar with ternary blends. Comput Concr 21(2):149–156

Turk K, Karatas M, Gonen T (2013) Effect of Fly Ash and Silica Fume on compressive strength, sorptivity and carbonation of SCC. KSCE J Civ Eng 17(1):202–209

Turk K, Kina C, Bagdiken M (2017) Use of binary and ternary cementitious blends of F-Class fly-ash and limestone powder to mitigate alkali-silica reaction risk. Constr Build Mater 151:422–427

Turk K, Kina C, Oztekin E (2020) Effect of macro and micro fiber volume on the flexural performance of hybrid fiber reinforced SCC. Adv Concr Constr 10(3):257–269

Turk K, Bassurucu M, Bitkin RE (2021) Workability, strength and flexural toughness properties of hybrid steel fiber reinforced SCC with high-volume fiber. Constr Build Mater 266:120944

Turk K, Oztekin E, Kina C (2022) Self-compacting concrete with blended short and long fibres: experimental investigation on the role of fibre blend proportion. Eur J Environ Civ Eng 26(3):905–918

Türk K, Kına C (2017) Çimento esasli kompozitlerde karma lif kullanimı. Pamukkale Üniversitesi Mühendislik Bilimleri Dergisi 23(6):671–678

Uysal M, Tanyildizi H (2012) Estimation of compressive strength of self compacting concrete containing polypropylene fiber and mineral additives exposed to high temperature using artificial neural network. Constr Build Mater 27(1):404–414

Uysal M, Yilmaz K, Ipek M (2012) The effect of mineral admixtures on mechanical properties, chloride ion permeability and impermeability of self-compacting concrete. Constr Build Mater 27(1):263–270

Vapnik VN (1999) An overview of statistical learning theory. IEEE Trans Neural Netw 10(5):988–999

Wongkeo W, Thongsanitgarn P, Ngamjarurojana A, Chaipanich A (2014) Compressive strength and chloride resistance of self-compacting concrete containing high level fly ash and silica fume. Mater Des 64:261–269

Wu W, Wang R, Zhu C, Meng Q (2018) The effect of fly ash and silica fume on mechanical properties and durability of coral aggregate concrete. Constr Build Mater 185:69–78

Xiao H, Duan Z, Zhou Y, Zhang N, Shan Y, Lin X, Liu G (2019) CO2 emission patterns in shrinking and growing cities: a case study of Northeast China and the Yangtze River Delta. Appl Energy 251:113384

Yaseen ZM, Deo RC, Hilal A, Abd AM, Bueno LC, Salcedo-Sanz S, Nehdi ML (2018) Predicting compressive strength of lightweight foamed concrete using extreme learning machine model. Adv Eng Softw 115:112–125

Yuvaraj P, Ramachandra Murthy A, Iyer NR, Sekar SK, Samui P (2013) Support vector regression based models to predict fracture characteristics of high strength and ultra high strength concrete beams. Eng Fract Mech 98(1):29–43

Zhang D, Tsai JJP (2003) Machine learning and software engineering. Softw Qual J 11(2):87–119

Zhou T, Wang F, Yang Z (2017) Comparative analysis of ANN and SVM models combined with wavelet preprocess for groundwater depth prediction. Water (switzerland) 9(10):781

Springer Nature or its licensor (e.g. a society or other partner) holds exclusive rights to this article under a publishing agreement with the author(s) or other rightsholder(s); author self-archiving of the accepted manuscript version of this article is solely governed by the terms of such publishing agreement and applicable law.